NEOCLASSICAL TRANSPORT IN URAGAN-2M FOR THE $1/\nu$ REGIME

B. SEIWALD* *Graz University of Technology, Institute of Theoretical and Computational Physics*
Petersgasse 16, A–8010 Graz, Austria

V. N. KALYUZHNYJ and S. V. KASILOV
National Science Center "Kharkov Institute of Physics and Technology"
Institute of Plasma Physics, Akademicheskaya Str. 1, 61108 Kharkov, Ukraine

W. KERNBICHLER *Graz University of Technology, Institute of Theoretical and Computational Physics*
Petersgasse 16, A–8010 Graz, Austria

V. V. NEMOV *National Science Center "Kharkov Institute of Physics and Technology"*
Institute of Plasma Physics, Akademicheskaya Str. 1, 61108 Kharkov, Ukraine

Received November 21, 2005
Accepted for Publication April 3, 2006

In the framework of optimization of confinement properties of Uragan-2M, neoclassical transport in the $1/\nu$ regime and the pertinent stored energy are studied. A rather wide range of device configurations is considered. For the computations the field line following code NEO for computation of transport measures is used. Computations are performed in real-space coordinates using the magnetic field produced by the device coils. The difference of currents in adjacent groups of toroidal field (TF) coils as well as the current in the TF coils and the additional vertical magnetic field are used as varying parameters.

Some possibilities for improving the $1/\nu$ transport corresponding to optimum values of the varying parameters are presented.

KEYWORDS: *stellarator optimization, neoclassical transport, Uragan-2M*

I. INTRODUCTION

The Uragan-2M (U-2M) device[1] is an $l = 2$ torsatron with an additional toroidal magnetic field. In the design phase of this device, various studies have been carried out. The results are summarized in Ref. 1. Because of the flexibility of the magnetic system of the device, further investigations of possibilities for an improvement of confinement properties are possible and desirable.

Numerical calculations of the $1/\nu$ transport (effective ripple, ϵ_{eff}) are of big importance for assessing the general confinement properties of the device. Here, the $1/\nu$ neoclassical transport is studied for U-2M using the field line following code NEO (Ref. 2) for computation of transport measures. Additionally, an optimizing procedure with respect to the stored energy in the $1/\nu$ regime is carried out using the SORSSA code[3] for optimizing stellarators with fixed coil design. According to the general concept of stellarator optimization,[4] just the $1/\nu$ regime of transport in stellarators should be optimized. The $1/\nu$ transport is characterized by the effective (or equivalent helical) ripple ϵ_{eff}. It follows from Ref. 4 that for the W7-X configuration, which is well optimized, this ripple is $\sim$1.5%. For new optimized stellarator devices [e.g., HSX (Ref. 5), NCSX (Ref. 6), CHS-qa (Ref. 7)], conditions corresponding to such or even smaller values of ϵ_{eff} have been a design goal. For existing stellarators, a decrease of ϵ_{eff} can be achieved by changes in coil currents. As examples, inwardly shifted conffigurations[8–10] for CHS and LHD can be quoted. With such a shift so-called σ optimized configurations[11] can be achieved. The inwardly shifted configuration is favorable for drift orbit optimization, but formation of a magnetic hill instead of a magnetic well is possible. Nevertheless, it follows from experimental results[8,10] for CHS and LHD that magnetohydrodynamic stability and good transport properties are compatible in the inwardly shifted configuration.

For optimizing the energy confinement, the plasma volume is included in the criterion for the optimization.

*E-mail: Bernhard.Seiwald@itp.tugraz.at

The energy content is directly linked to the energy confinement time, which is one of the main characteristics of an experimental device. If one optimizes an existing device with a fixed coil system and limitation due to the vacuum vessel, it should be always kept in mind that the improvement of the transport coefficients can be achieved at the expense of the loss of plasma volume. The total effect of optimization on the energy confinement time might then be negative; for this reason, an inward shift of the configuration that leads to a reduction of transport coefficients may lead also to a reduction of plasma volume and, therefore, has to be limited by a certain compromise value. It can be checked by varying temperature at the plasma boundary, that the energy content is weakly sensitive to this value as long as the core plasma is deeply in a collisionless regime and, therefore, the influence of outer regions where plateau or Pfirsch-Schlüter regimes are important, is small. A relatively simple parameter like the energy content in the $1/\nu$ regime allows one to limit the scope of optimization to the optimization of the magnetic field geometry, which is a demanding problem from the viewpoint of the computer time.

The presented computations are performed for magnetic fields produced by the coils of the U-2M magnetic system without taking into account the current-feeds and detachable joints of the helical winding. For this study the currents in adjacent pairs of toroidal field (TF) coils are varied.[12] In addition, possibilities for improving the neoclassical transport by changing the value of the current in the TF coils and by changing the resulting vertical magnetic field are considered.

II. BASIC PARAMETERS

The magnetic system of U-2M is basically defined by the big radius of the torus with $R_T = 170$ cm and by the number of field periods along the torus with $n_p = 4$. The additional toroidal magnetic field in U-2M is produced by a system of 16 TF coils uniformly distributed in angle along the major circumference (four coils in each field period). The mean current in such a coil, I_{TFC}, is expressed in units of the helical winding current. In accordance with Ref. 1 for the standard configuration, this current is $I_{TFC} = 5/12$. In this case the parameter $k_\varphi = B_{th}/(B_{th} + B_{tt})$ is $k_\varphi = 0.375$, where B_{th} and B_{tt} are the toroidal components of the magnetic field produced by the helical winding and TF coils, respectively. For the so-called fat configuration, the mean current in a TF coil is $\sim 9/14$ ($k_\varphi = 0.28$). The additional control parameter for improving the effective ripple is the difference of currents in adjacent pairs of TF coils.[1,12] An exact definition is given below.

The vertical field (VF) coil system plays an important role in formation of the magnetic configuration of the torsatron. The total vertical magnetic field $B_\perp$ is produced by the VF coils and the vertical magnetic field of the helical winding. The desired vertical field is achieved by adjusting the current in the VF coils. In the computations the VF coil system variant[13] is used, which allows one to suppress significantly the island structure of the magnetic surfaces.

The magnetic field produced by the helical winding and its spatial derivatives are calculated on the basis of the Biot-Savart law, where each helical coil is modeled with 24 current filaments distributed in two layers. The magnetic fields produced by the TF and VF coils are calculated using elliptic integrals (fields obtained in the local coordinate systems of each coil are transformed to general cylindrical coordinates). The model of the field used in the present work is somewhat incomplete since the influence of the current-feeds and detachable joints of the helical winding is not taken into account. Nevertheless, the model is close to realistic conditions and allows one to analyze possible ways for decreasing $1/\nu$ transport.

Preliminary computations of the magnetic field from each part of the coil system are performed separately on a three-dimensional grid to minimize computer time expenses for computations of the stored energy. For calculations of the stored energy, the magnetic fields are found using the Lagrange polynomial interpolation on this grid and superposition of the results.

Appropriate for the optimization are the following three control parameters, which are related to the currents in the helical winding and in TF as well as VF coils:

1. I_{TFC}, the mean current of TF coils, in units of helical winding current. It is directly connected to the aforementioned parameter k_φ (used in Refs. 1 and 12) by the ratio $k_\varphi = 1/(1 + 4I_{TFC})$ as it follows from the k_φ definition.
2. ΔI, which is introduced in view of the results of Ref. 12. The currents in the TF coils are presented further in a form $I_{TFC} \pm \Delta I$ with a plus sign for the inner two coils in each field period and with a minus sign for the outer two coils (ΔI is also expressed in units of the helical winding current).
3. f_{VFC}, a multiplying factor for the currents in the VF coils. This factor is connected to an additional vertical magnetic field. It enters linearly into the expression for the magnetic field of the VF coils in a way that for $k_\varphi = 0.375$ it results in $B_\perp/B_0 = 2.5\%$ for $f_{VFC} = 1$, $B_\perp/B_0 = 0$ for $f_{VFC} = 1.166$, and $B_\perp/B_0 = -2.5\%$ for $f_{VFC} = 1.332$. Here, $B_\perp$ is the resulting vertical magnetic field, and B_0 is the mean toroidal magnetic field.

III. COMPUTATIONS FOR CONFIGURATIONS WITH $k_\varphi = 0.375$

First computations are performed for the standard configuration ($k_\varphi = 0.375$, $I_{TFC} = 5/12$) with a resulting

vertical magnetic field $B_\perp$ of $B_\perp/B_0 \approx 2.5\%$. The standard configuration is well centered with respect to the vacuum chamber. For the used model of the helical winding (see Sec. II), the rotational transform changes from $\iota \approx 0.62$ (near the magnetic axis) to $\iota \approx 0.8$.

III.A. Computations of effective ripple

It follows from Refs. 1 and 12 that for the U-2M standard configuration, the helical winding produces a significant "geometrical" toroidal mirror ripple along the magnetic field line (nearly 3% on axis), which is essentially larger than the geometrical helical ripple near the axis. This results in rather large ϵ_{eff} on axis (~5%). Using differing currents in adjacent pairs of TF coils had been proposed in Ref. 12 for improving this result. As follows from Ref. 12, a proper alteration of the currents results in a nearly vanishing toroidal mirror term and leads to an essential decrease in ϵ_{eff} (see also Ref. 1).

In contrast to Ref. 12, here, this way of optimization is analyzed using methods[2] that are valid in entire magnetic configurations. In Ref. 12 a decrease in the effective ripple was found for U-2M for certain values of $\Delta I > 0$ and an increase for the case when $\Delta I < 0$. Here, the dependence of the effective ripple ϵ_{eff} on ΔI is analyzed using methods described in Ref. 2. It should be noted that the usage of $\epsilon_{eff}^{3/2}$ gives a better figure of merit than ϵ_{eff} since for the $1/\nu$ transport regime, the transport coefficients are proportional to $\epsilon_{eff}^{3/2}$ directly. For computing $\epsilon_{eff}^{3/2}$ the following expressions[2] are used:

$$\epsilon_{eff}^{3/2} = \frac{\pi R^2}{8\sqrt{2}} \lim_{L_s\to\infty}\left(\int_0^{L_s}\frac{ds}{B}\right)\left(\int_0^{L_s}\frac{ds}{B}\,|\nabla\psi|\right)^{-2} \times \int_{B_{min}^{(abs)}/B_0}^{B_{max}^{(abs)}/B_0} db' \sum_{j=1}^{j_{max}} \frac{\hat{H}_j^2}{\hat{I}_j} \quad , \tag{1}$$

$$\hat{H}_j = \frac{1}{b'}\int_{s_j^{(min)}}^{s_j^{(max)}} \frac{ds}{B}\sqrt{b' - \frac{B}{B_0}}\left(4\,\frac{B_0}{B} - \frac{1}{b'}\right)|\nabla\psi|\,k_G \quad , \tag{2}$$

and

$$\hat{I}_j = \int_{s_j^{(min)}}^{s_j^{(max)}} \frac{ds}{B}\sqrt{1 - \frac{B}{B_0 b'}} \quad , \tag{3}$$

where

B_0 = reference magnetic field

ψ = magnetic surface label

R = major radius of the torus

$k_G = (\mathbf{h}\times(\mathbf{h}\cdot\nabla)\mathbf{h})\cdot\nabla\psi/|\nabla\psi|$ = geodesic curvature of a magnetic field line with the unit vector $\mathbf{h} = \mathbf{B}/B$.

The quantity $\epsilon_{eff}^{3/2}$ is calculated by integration over the magnetic field line length s, over the sufficiently large interval $[0, L_s]$, and by integration over the perpendicular adiabatic invariant of trapped particles $J_\perp$ by means of the variable b'. In Eq. (1), $B_{min}^{(abs)}$ and $B_{max}^{(abs)}$ are the minimum and maximum values of B within the interval $[0, L_s]$.The quantities $s_j^{(min)}$ and $s_j^{(max)}$ within the sum over j in Eqs. (2) and (3) correspond to the turning points of trapped particles. Note that for the classical stellarator model,[14] ϵ_{eff} calculated with help of formula (1) coincides with the helical ripple ϵ_h.

Figure 1 shows cross sections of magnetic surfaces for $\Delta I = 0$ in the $\varphi = 0$ plane and after half of the field period. A circle with a radius of 34 cm shows the inner boundary of the vacuum chamber. A magnetic field line, which forms an island and belongs to a stochastic zone or a near-rational flux surface, is marked "field line with error code." These marked field lines are not used for computations of the total stored energy (see Sec. III.B). Nevertheless, they are shown to obtain as realistic a picture of the cross section as possible. Magnetic islands with rotational transform $\iota = 4/5$ can be seen close to the chamber boundary. Islands of such a kind had been already observed in Ref. 15. Cross sections for $\Delta I = 5/144$ and $\Delta I = -5/144$ differ from those in Fig. 1 mainly by the respective sizes of the outermost magnetic surfaces and, therefore, are not shown. For $\Delta I > 0$ ($\Delta I < 0$), these sizes are smaller (bigger) than those in Fig. 1. The positions of the islands for these magnetic configurations differ only slightly from that for $\Delta I = 0$. For $\Delta I = 5/144$ in the region outside the $\iota = 4/5$ islands, the magnetic configuration has entirely a structure of island chains consisting of very big numbers of small islands.

Results of computations of $\epsilon_{eff}^{3/2}$ for $\Delta I = 0$ and $\pm 5/144$ are presented in Fig. 2 for non-island magnetic surfaces as functions of the mean radius r of a magnetic surface. This mean radius is calculated as $r = r_{eff}$ using the formula[3]

$$r_{eff} = \frac{2}{3}\lim_{L_s\to\infty}\left(\int_0^{L_s}\frac{ds}{B}\,\mathbf{r}\cdot\nabla\psi\right)\left(\int_0^{L_s}\frac{ds}{B}\,|\nabla\psi|\right)^{-1} \quad . \tag{4}$$

The curves presented in Fig. 2 show gaps corresponding to regions with islands. Different total ranges of r_{eff} correspond to different sizes of the outermost magnetic surfaces. For $\Delta I = 5/144$, the $\epsilon_{eff}^{3/2}$ values at the inner flux surfaces are smaller by one order of magnitude than those for $\Delta I = 0$. However, this difference vanishes when approaching the vicinity of the islands. For $\Delta I = -5/144$, the $\epsilon_{eff}^{3/2}$ values are bigger than for $\Delta I = 0$. It also follows from the computations that $\epsilon_{eff}^{3/2}$ reaches the values 0.2 to 0.3 in the islands for all examined configurations. The obtained results are in qualitative agreement with the results of Ref. 12 for rather small r/a, with a being the mean radius of the outermost magnetic surface. The rather large $\epsilon_{eff}^{3/2}$ values of 0.01 to 0.1 ($\epsilon_{eff} \approx 0.05$ to 0.22)

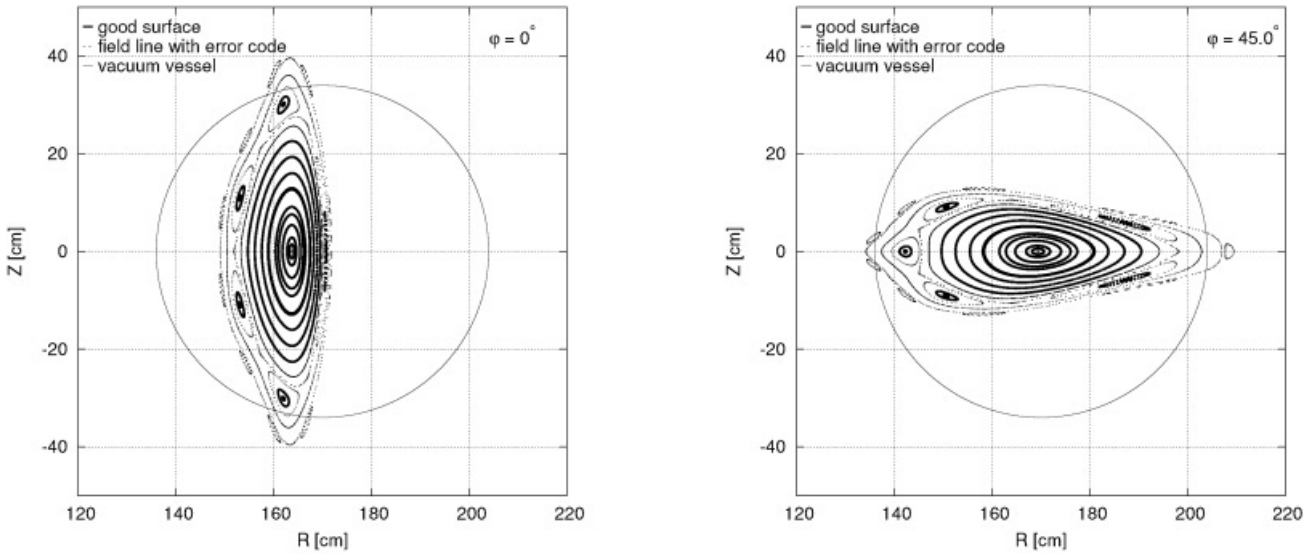

Fig. 1. Standard configuration of U-2M for $\Delta I = 0$ ($B_\perp/B_0 = 2.5\%$).

are characteristic in the range from $r_{eff} \approx 7$ cm up to the island position. An increase in $\epsilon_{eff}^{3/2}$ for the island surfaces indicates that inside the magnetic islands, local magnetic configurations are formed for which the confinement properties can differ from those for the basic non-island surfaces.

Another way for decreasing the $1/\nu$ transport in stellarators with helical windings is connected to inwardly-shifted configurations (see, e.g., Refs. 8 and 10). To achieve inwardly-shifted configurations, the resulting vertical magnetic field has to be modified in a certain way. In addition to $B_\perp/B_0 \approx 2.5\%$, calculations are performed for $B_\perp = 0$ and $B_\perp/B_0 \approx -2.5\%$ for $\Delta I = 0$. The positive (negative) $B_\perp$ value corresponds to the somewhat undercompensated (overcompensated) vertical field of the helical winding. Two different scenarios of these modifications have been studied. In the first case an additional homogeneous vertical magnetic field of the necessary value is used. This is an idealized case and the simplest way for obtaining the desirable configurations. In the second case, which is closer to the practice of experiments, the necessary $B_\perp/B_0$ value is obtained by increasing the currents of the VF coils instead of using the additional homogeneous magnetic field. Because of the changes in $B_\perp/B_0$, the magnetic axis turns out to be inwardly shifted with respect to its position for $B_\perp/B_0 = 2.5\%$. Figures 3 and 4 show magnetic surfaces corresponding to the modifications in $B_\perp$ obtained by increasing the currents in the VF coils for $B_\perp/B_0 = 0$ and $B_\perp/B_0 = -2.5\%$. These pictures differ only slightly from analogous pictures where the additional homogeneous vertical magnetic field is used.

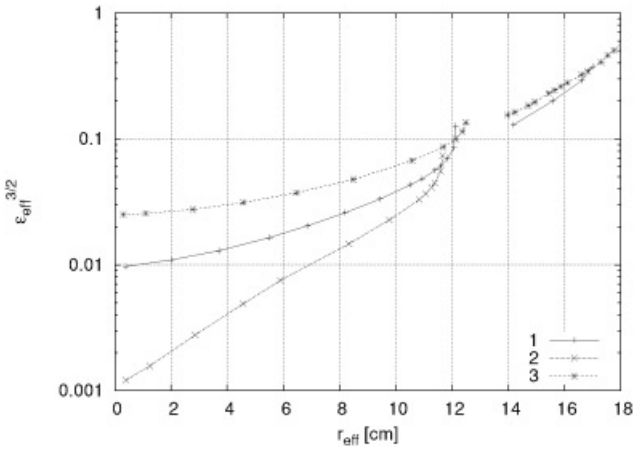

Fig. 2. Parameter $\epsilon_{eff}^{3/2}$ as a function of r_{eff} for various ΔI; 1: $\Delta I = 0$; 2: $\Delta I = 5/144$; 3: $\Delta I = -5/144$ (gaps in curves correspond to the island surfaces).

Computational results for $\epsilon_{eff}^{3/2}$ corresponding to the new values of $B_\perp/B_0$ for the configurations obtained for the increased currents in the VF coils are presented in Fig. 5 (curves 1 and 2). These results are very close to the analogous results obtained in the case of using the additional vertical homogeneous magnetic field, which are not presented in Fig. 5. For better comparison Fig. 5 also shows some results from Fig. 2 (curves 3 and 4).

It follows from Fig. 5 that the new magnetic configurations have markedly smaller values of the effective ripple than the configurations with $B_\perp/B_0 = 2.5\%$. To comment on these results, some plots of B along field lines corresponding to $r_{eff} \approx 11.5$ to 12 cm are shown in Fig. 6. Together with features corresponding to the toroidal and helical inhomogeneities of B, frequent small

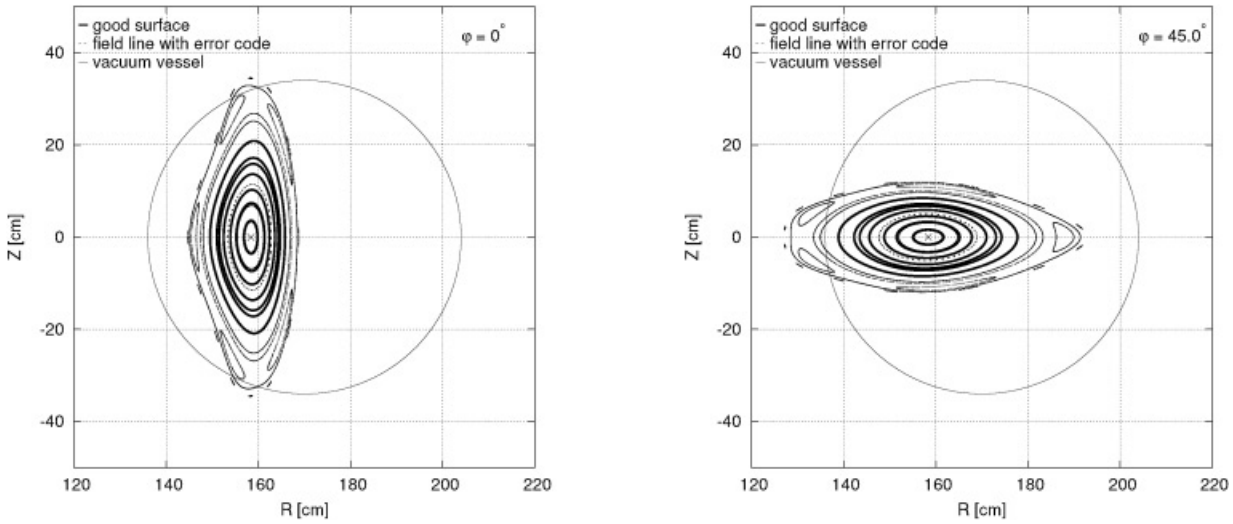

Fig. 3. Configuration of U-2M ($k_\varphi = 0.375$) for $\Delta I = 0$ and $B_\perp/B_0 = 0$.

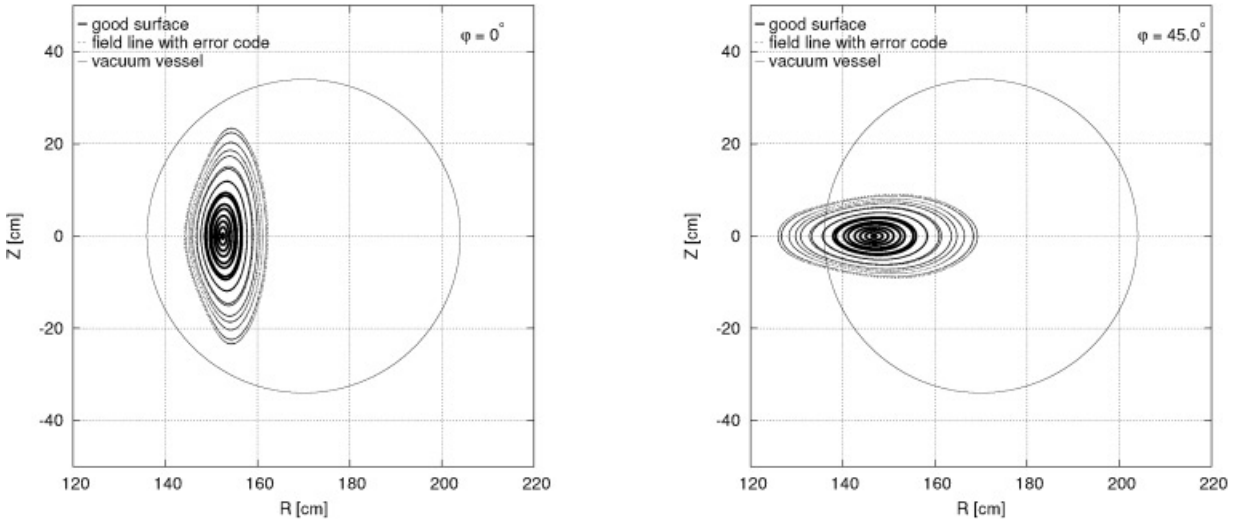

Fig. 4. Configuration of U-2M ($k_\varphi = 0.375$) for $\Delta I = 0$ and $B_\perp/B_0 = -2.5\%$.

ripples from the TF coils are seen in the plots. From Fig. 5, it follows that B for the standard configuration ($B_\perp/B_0 \approx 2.5\%$), which has the highest transport, in some measure resembles B corresponding to an opposite case of the σ optimized configuration.[11] This correlates with the fact that the standard configuration is actually a configuration with an outwardly shifted magnetic axis and corresponds to an enhanced radial ∇B drift of locally trapped particles. This is unfavorable from the viewpoint of $1/\nu$ transport. Slight improvement can be achieved only for the inner region by alteration of the TF coil currents,[12] as is shown above. The configuration corresponding to $B_\perp = 0$ is actually not an inwardly shifted one but is a configuration for which the vertical field of the helical winding is fully compensated. The B plot differs markedly from that for the configuration with $B_\perp/B_0 \approx 2.5\%$. The $\epsilon_{eff}^{3/2}$ results are close to the analogous results for the stellarator field corresponding to one toroidal harmonic in Ref. 2. The minimum of $\epsilon_{eff}^{3/2}$ is obtained for $B_\perp/B_0 \approx -2.5\%$. This corresponds to an inwardly shifted configuration, but σ optimization[11] is not reached in this case as is seen from the plot of B in Fig. 6. The condition of nearly the same B values for all minima of the helical ripples is not fulfilled. With further increase of the inward shift, σ optimization might be realized, but such a shift has no relevance for U-2M because of a strong limitation of the plasma volume by the vacuum chamber.

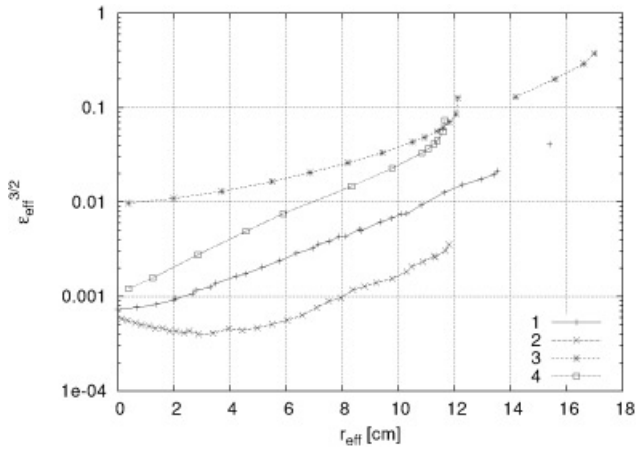

Fig. 5. Parameter $\epsilon_{eff}^{3/2}$ as a function of r_{eff} for various $B_\perp/B_0$; 1: $\Delta I = 0$, $B_\perp = 0$; 2: $\Delta I = 0$, $B_\perp/B_0 = -2.5\%$; 3: $\Delta I = 0$, $B_\perp/B_0 = 2.5\%$; 4: $\Delta I = 5/144$, $B_\perp/B_0 = 2.5\%$.

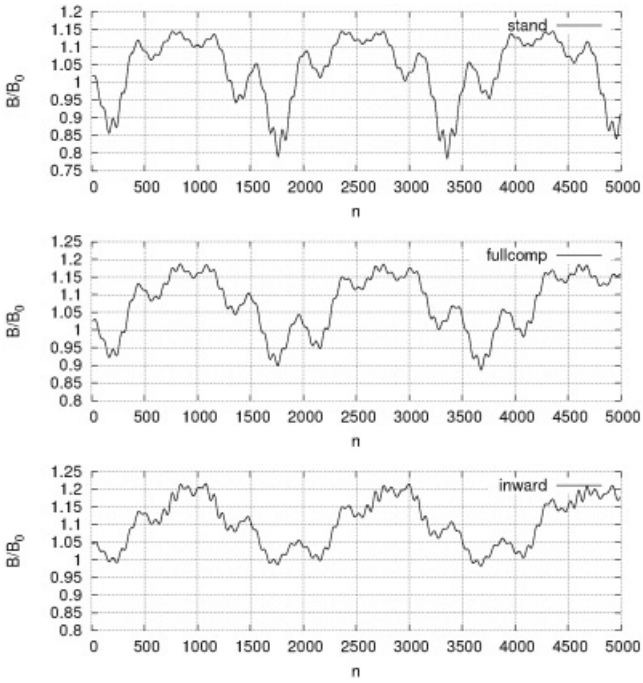

Fig. 6. Variation of the magnetic field strength along the magnetic field line for three configurations corresponding to $k_\varphi = 0.375$: (top) $B_\perp/B_0 = 2.5\%$, $r_{eff} = 11.35$ cm, $\iota = 0.753$; (middle) $B_\perp/B_0 = 0$ (fully compensated vertical field), $r_{eff} = 12.03$ cm, $\iota = 0.634$; (bottom) $B_\perp/B_0 = -2.5\%$ (inwardly shifted), $r_{eff} = 11.43$ cm, $\iota = 0.68$.

Actually, the confinement regions are smaller than those seen from Figs. 2 and 5 because of islands and the restrictions by the vacuum chamber. The regions where confinement is achieved can be characterized by the corresponding maximum values of r_{eff}, which equal $r_{eff} \approx 15.4$ cm for $B_\perp = 0$, $r_{eff} \approx 11.8$ cm for $B_\perp/B_0 = -2.5\%$, and $r_{eff} \approx 11.7$ for $B_\perp/B_0 = 2.5\%$, $\Delta I = 5/144$.

In Figs. 2 and 5, only results for typical cases are shown. The detailed parameter survey is presented in Figs. 12 and 13.

III.B. Optimization of Energy Confinement

In Ref. 3 an optimization procedure for the stored energy in the plasma was worked out to analyze the confinement properties of the TJ-II device[16] in the $1/\nu$ regime. The code for optimization uses the NEO code[2] for the calculations of the heat conductivity $\kappa_\perp$. This procedure is used for analogous computations for U-2M.

In the procedure the total stored energy in the plasma volume is used as a figure of merit with an energy source localized at the magnetic axis, $Q(r) = (Q_0/r)\delta(r)$. It is assumed that the temperature profile is defined by the heat conductivity equation

$$\frac{1}{r}\frac{d}{dr} r\kappa_\perp \frac{dT}{dr} + Q(r) = 0 \ , \tag{5}$$

with the boundary conditions $T(a) = 0$ and $\lim_{r\to 0}(r(dT/dr)) = 0$, where a is the boundary of the plasma. The heat conductivity is proportional to $\epsilon_{eff}^{3/2} T^{7/2}$, and computation of $\epsilon_{eff}^{3/2}$ for sets of computed magnetic surfaces is an essential part of the optimization procedure. The normalized stored energy

$$\hat{W} = \int_0^a dr\, r\hat{n}(r) \left(\int_r^a \frac{dr'}{r'\epsilon_{eff}^{3/2}(r')} \right)^{2/9} \tag{6}$$

can be obtained by integrating the temperature profile resulting from Eq. (5), where $\hat{n}$ is the normalized plasma density. The energy content W scales with $\hat{W}$ and device parameters as follows:

$$W = CP^{2/9} B_0^{4/9} R^{11/9} n_0 \hat{W} \ , \tag{7}$$

where P and n_0 are total input power and central density, respectively, and C is a constant that is weakly dependent (via a Coulomb logarithm) on the plasma parameters.

It should be noted that the energy content is weakly sensitive to the temperature T_a at the plasma boundary. In the presented model T_a is fixed to $T_a = 0$. As long as T_a does not exceed 50% of the temperature at half of the plasma radius, the energy content changes $<5\%$. Therefore, the main energy content comes from the regions where $1/\nu$ transport is still dominant.

First, computations are performed for the standard configuration as well as for configurations where the parameter ΔI is varied within the interval $[-0.1, 0.1]$. The results, corresponding to models where constant and parabolic profiles $[\hat{n} = 1 - \alpha(r/a)^2$, with $\alpha = 0.8]$ for the particle density are assumed, are presented in Fig. 7 in form of the renormalized stored energy,

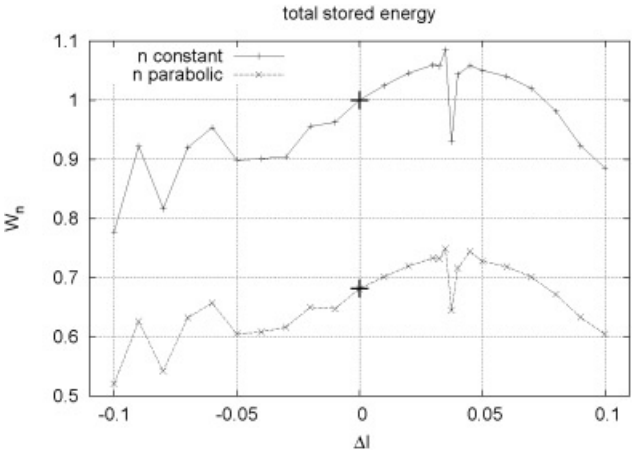

Fig. 7. Renormalized stored energy [see Eqs. (6) and (8)] for $B_\perp/B_0 = 2.5\%$ versus change of ΔI.

$$W_n = \hat{W}/\hat{W}_S \ , \tag{8}$$

as a function of ΔI, with $\hat{W}_S$ the normalized stored energy for the standard configuration and the constant particle density profile. As it turned out in Ref. 3 the energy for the model with parabolic particle density scales as 0.7 of $\hat{W}$ for the constant particle density profile. Hence, the model for the particle density $\hat{n} = const$ is used for all other computations of the total stored energy. A maximum in the stored energy is seen for $\Delta I \approx 0.035$, which is rather close to $\Delta I = 5/144$ considered above. Surfaces outside the islands are not fully inside the vacuum vessel and, therefore, suppressed for computations of the total stored energy (nevertheless $\epsilon_{eff}^{3/2}$ is shown for such surfaces for ΔI equal to 0 and $-5/144$ in Fig. 2). Close to the configuration with a maximum in the stored energy, a configuration with markedly smaller energy is seen for $\Delta I = 0.0375$. For this configuration the plasma radius is significantly smaller than for the neighboring configurations because of islands and stochastic zones.

Further, calculations are performed for $\Delta I = 0$ with the changed value of $B_\perp$ corresponding to inwardly shifted configurations. Again, as described at the end of Sec. III.A, the inward shift can be obtained by either an additional homogeneous vertical field or an increase of the currents in the VF coils. Because of the small difference, the following calculations are performed only for the case of increasing the currents in the VF coils.

The study of $\hat{W}$ turned out to be convenient for W_n being a function of f_{VFC} within the interval [1, 1.332], where f_{VFC} is connected to $B_\perp$ in a way indicated in Sec. II. In this and Sec. III, the consequence of the limitation of the usable plasma volume by the vacuum vessel is briefly discussed for various configurations. The total stored energy is presented in Fig. 8 for computations where the limitation due to the vacuum chamber is taken into account as well as for computations where it is ignored. Taking into account this limitation of the plasma volume, an optimum value of the vertical magnetic field has been found. The maximum of the stored energy is approximately $1.5/1.06 \approx 1.4$ times bigger than the corresponding maximum in Fig. 7, where ΔI is the varying parameter. The optimum f_{VFC} corresponds to $B_\perp/B_0 \approx 0$ and is determined by opposite effects of decreasing neoclassical transport coefficients and increasing limitation due to the vacuum chamber for increasing inward shift of the plasma. For the case when ignoring the limitation, the maximum in the stored energy is higher and is realized for f_{VFC} close to a value corresponding to $B_\perp/B_0 \approx -2.5\%$.

IV. CONFIGURATIONS WITH DECREASED PARAMETER k_φ

The flexibility of the magnetic system of U-2M allows operating in regimes with decreased parameter k_φ. Decreasing this parameter, compared to its value for the standard configuration, corresponds to some increase of the ratio of the total toroidal magnetic field to the field produced by the helical winding. This may reduce the helical ripple and increase the confinement volume of the configuration if the limitation due to the vacuum chamber is not taken into account. Both of these factors may lead to an improvement of the stored energy in the $1/\nu$ transport regime. In addition, decreasing k_φ can also be useful in U-2M for reducing the magnetic island structure produced by current-feeds and detachable joints of the helical winding (see, e.g., Refs. 17 and 18). Note that reduction of k_φ decreases also the rotational transform in the confinement region.

Because of these reasons it is of interest to study the $1/\nu$ transport for decreased values of k_φ. Such a study is performed in the present section for k_φ in the range of

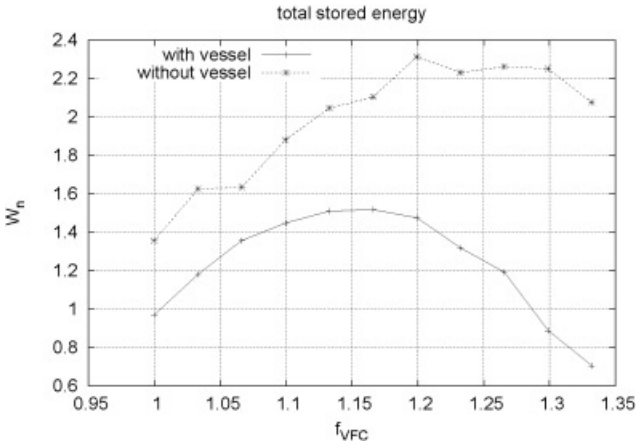

Fig. 8. Renormalized stored energy [see Eqs. (6) and (8)] for $\Delta I = 0$ versus change of $B_\perp/B_0$ (f_{VFC}) with the limitation by the chamber ("with vessel") and neglecting this limitation ("without vessel").

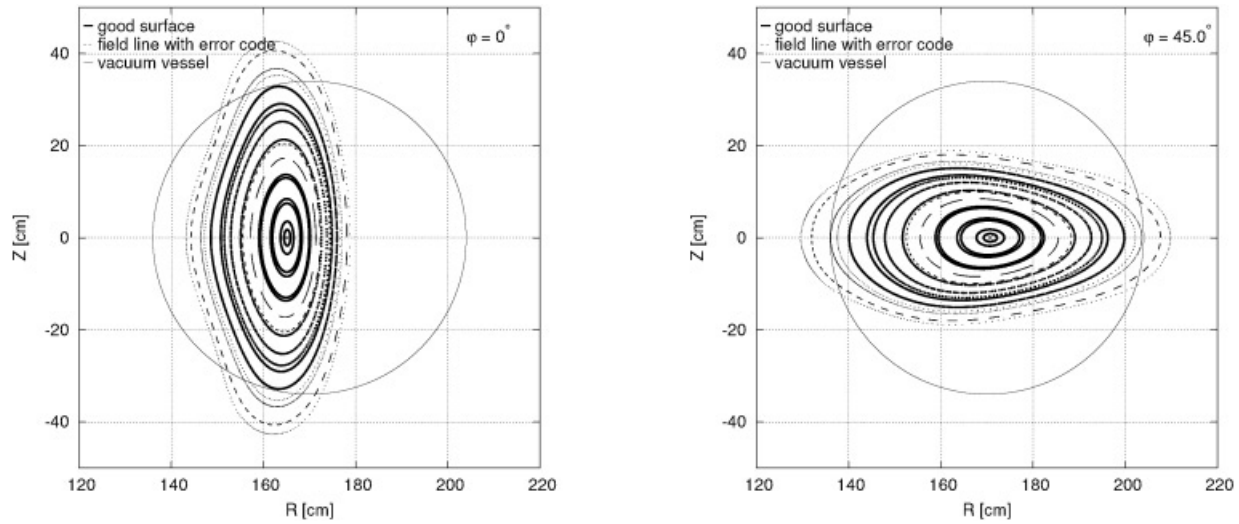

Fig. 9. Magnetic configuration of U-2M for $k_\varphi = 0.31$ ($I_{TFC} = 5/9$) and $f_{VFC} = 1$ ($B_\perp/B_0 \approx 2.07\%$).

$k_\varphi = 0.28$ corresponding to the fat configuration to $k_\varphi = 0.375$. The parameter f_{VFC} (connected to $B_\perp$) is varied in the same way as described at the end of Sec. III.B. Most calculations are performed for $\Delta I = 0$ (identical currents in the TF coils) except for the case discussed at the end of this section.

As an example, Fig. 9 shows magnetic surfaces corresponding to $k_\varphi \approx 0.31$ for $f_{VFC} = 1$, i.e., with the same $B_\perp$ as for the standard configuration. It can be seen from Fig. 9 that good magnetic surfaces fill up the vacuum chamber to a larger extent than those for the standard configuration in Fig. 1. Figure 10 illustrates the dependence of effective radius r_{eff}, calculated using formula (4), of the outermost magnetic surface limited by the chamber, on the f_{VFC} parameter for $k_\varphi \approx 0.31$ and $k_\varphi = 0.375$. It can be seen that for both values of k_φ, the effective radius decreases when shifting the configurations inward. The usable plasma volume is limited for $k_\varphi = 0.375$ and f_{VFC} close to one by islands and stochastic zones.

For most values of f_{VFC}, the effective ripple is found to be somewhat smaller than for $k_\varphi = 0.375$. Figure 11 shows the results for $\epsilon_{eff}^{3/2}$ corresponding to $k_\varphi \approx 0.31$ in cases of $f_{VFC} = 1$ and 1.166. The latter value corresponds to full compensation of the mean vertical magnetic field of the helical winding. In addition, curve 3 shows the results corresponding to $\Delta I \neq 0$ ($f_{VFC} = 1$, $k_\varphi \approx 0.31$), which are discussed at the end of this section. For comparison, the results for the standard configuration ($f_{VFC} = 1$, $\Delta I = 0$) are shown. Some improvement of flux surfaces also takes place for the magnetic surfaces within the part of the magnetic configuration limited by the chamber, as is seen from Figs. 9 and 10.

The described strategies should lead to an increase in the stored energy. Figures 12 and 13 present the results of computations for this quantity. Figure 12 relates to computations with taking into account the limitations of the plasma volume due to the vacuum chamber, which are neglected in Fig. 13. The presented results are obtained for various values of I_{TFC} and f_{VFC} used as varying parameters within the limits of $1 \leq f_{VFC} \leq 1.332$ and $5/12 \leq I_{TFC} \leq 9/14$. Together with I_{TFC} the values of k_φ connected to this parameter (see Sec. II) are also presented in the captions of Figs. 12 and 13. It follows from Figs. 12 and 13 that with decreasing k_φ the stored energy

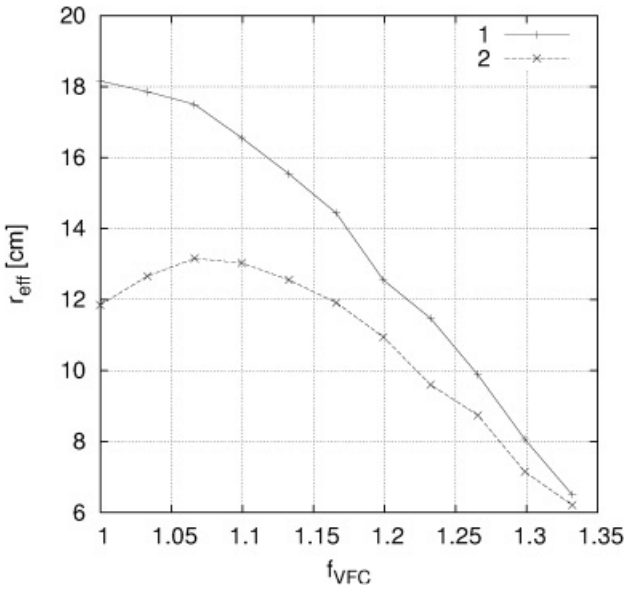

Fig. 10. Effective radius of the outermost magnetic surface (within the chamber) versus change of f_{VFC} ($B_\perp/B_0$); 1: $k_\varphi = 0.31$; 2: $k_\varphi = 0.375$.

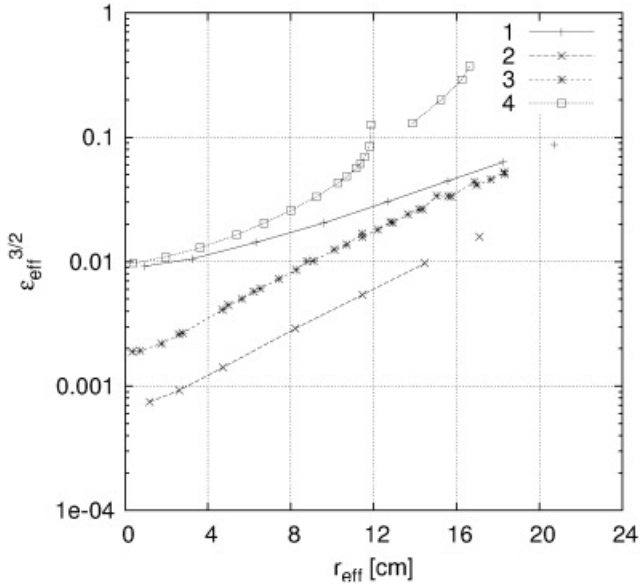

Fig. 11. Parameters $\epsilon_{eff}^{3/2}$ as functions of r_{eff} for $k_\varphi = 0.31$ and various f_{VFC}; 1: $f_{VFC} = 1$, $\Delta I = 0$; 2: $f_{VFC} = 1.166$ $(B_\perp/B_0 = 0)$, $\Delta I = 0$; 3: $f_{VFC} = 1$, $\Delta I = 0.06$; 4 (standard configuration): $k_\varphi = 0.375$, $f_{VFC} = 1$, $\Delta I = 0$ (see Fig. 2, curve 1).

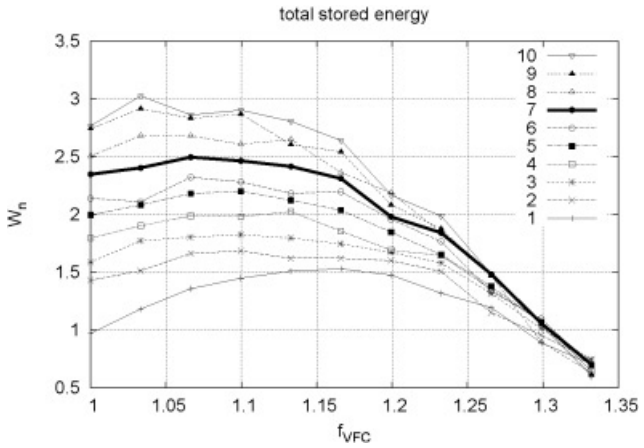

Fig. 12. Renormalized stored energy [see Eqs. (6) and (8)] for various f_{VFC} $(B_\perp/B_0)$ and I_{TFC} (k_φ) with taking into account limitations by the chamber; 1: $I_{TFC} = 0.41667$ $(k_\varphi = 0.375)$; 2: $I_{TFC} = 0.43928$ $(k_\varphi = 0.33627)$; 3: $I_{TFC} = 0.4619$ $(k_\varphi = 0.3512)$; 4: $I_{TFC} = 0.4845$ $(k_\varphi = 0.3404)$; 5: $I_{TFC} = 0.5071$ $(k_\varphi = 0.3302)$; 6: $I_{TFC} = 0.5298$ $(k_\varphi = 0.3206)$; 7: $I_{TFC} = 0.55555$ $(k_\varphi = 0.3103)$; 8: $I_{TFC} = 0.5976$ $(k_\varphi = 0.2949)$; 9: $I_{TFC} = 0.62024$ $(k_\varphi = 0.2873)$; 10: $I_{TFC} = 0.6429$ $(k_\varphi = 0.28)$.

increases, and the maxima in the stored energy correspond to some optimum values of f_{VFC} $(B_\perp)$.

The results corresponding to $I_{TFC} = 5/9$ $(k_\varphi \approx 0.31)$ are of special interest because it follows from Ref. 18 that

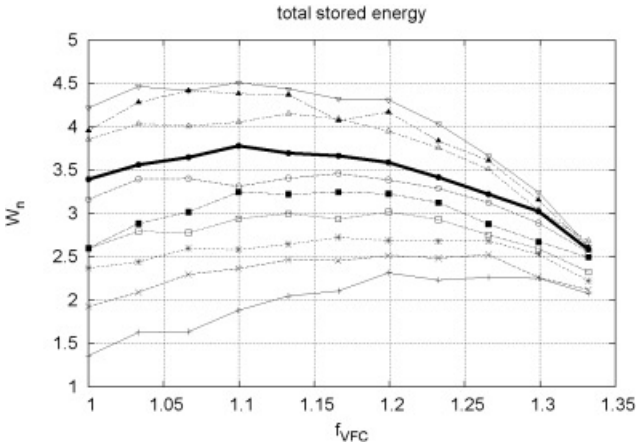

Fig. 13. Renormalized stored energy [see Eqs. (6) and (8)] for various f_{VFC} $(B_\perp/B_0)$ and I_{TFC} (k_φ) with neglecting limitations by the chamber; 1: $I_{TFC} = 0.41667$ $(k_\varphi = 0.375)$; 2: $I_{TFC} = 0.43928$ $(k_\varphi = 0.33627)$; 3: $I_{TFC} = 0.4619$ $(k_\varphi = 0.3512)$; 4: $I_{TFC} = 0.4845$ $(k_\varphi = 0.3404)$; 5: $I_{TFC} = 0.5071$ $(k_\varphi = 0.3302)$; 6: $I_{TFC} = 0.5298$ $(k_\varphi = 0.3206)$; 7: $I_{TFC} = 0.55555$ $(k_\varphi = 0.3103)$; 8: $I_{TFC} = 0.5976$ $(k_\varphi = 0.2949)$; 9: $I_{TFC} = 0.62024$ $(k_\varphi = 0.2873)$; 10: $I_{TFC} = 0.6429$ $(k_\varphi = 0.28)$.

for $k_\varphi \approx 0.31$ the magnetic configuration of U-2M is less sensitive to the influence of current-feeds and detachable joints of the helical winding. It has been shown that in this case for the major part of the configuration, the rotational transform stays within the range $1/3 < \iota < 1/2$, and big magnetic islands are absent.

For $k_\varphi \approx 0.31$ (thick line in Fig. 12), it follows that the maximum in the stored energy is approximately $2.5/1.5 \approx 1.65$ times higher than the corresponding maximum for $k_\varphi = 0.375$ (Fig. 8). The optimum value for f_{VFC} ($f_{VFC} \approx 1.07$) is lower than the value for $k_\varphi = 0.375$ ($f_{VFC} \approx 1.166$) and corresponds to a higher value of $B_\perp/B_0$ ($B_\perp/B_0 \approx 1.19\%$). Note that for $k_\varphi \approx 0.31$, even without an additional inward shift ($f_{VFC} = 1$), the stored energy is higher than the maximum that can be achieved for $k_\varphi = 0.375$ (see Fig. 8). The stored energy is slightly lower than the maximum that is achieved for $f_{VFC} \approx 1.07$. Therefore, it is of interest to analyze the effect of changes of ΔI on the stored energy in absence of the additional inward shift of the magnetic configuration ($f_{VFC} = 1$).

For this study the corresponding computations for the stored energy have been carried out using ΔI as a varying parameter within the interval $[-0.1, 0.1]$ ($k_\varphi \approx 0.31, f_{VFC} = 1$). As a result for the optimum $\Delta I \approx 0.06$, the maximum of W_n is $\approx$2.64 when taking into account the limitation of the usable volume due to the chamber and $\approx$4.23 when neglecting this limitation. The stored energy is $2.64/2.5 \approx 1.056$ times higher than the maximum obtained for the inward shift of the magnetic surfaces for $\Delta I = 0$ (see Fig. 12, thick curve). The reason for such an improvement is a decreased effective ripple for the

optimum $\Delta I \approx 0.06$. These dependences of $\epsilon_{eff}^{3/2}$ on r for this optimum are shown in Fig. 11 with curve 3.

V. CONCLUSIONS

The standard configuration ($k_\varphi = 0.375$) with $B_\perp / B_0 \approx 2.5\%$ is well centered with respect to the vacuum chamber. Using a realistic model of the magnetic field and computational methods that allow investigations over the entire magnetic configuration shows an essentially high $1/\nu$ transport for this configuration.

Some possibilities for improving the $1/\nu$ confinement properties using optimization procedures for a set of three varying parameters have been presented. The parameters are connected to the TF coil currents, the difference of these currents in adjacent pairs of coils, and the changes in the vertical magnetic field.

Some improvement of the transport can be achieved for the standard configuration using a certain difference of currents in adjacent pairs of TF coils. Markedly lower $1/\nu$ transport can be obtained for inwardly-shifted configurations. Inward shifts lead to reduced usable plasma volumes because of the limitation due to the vacuum chamber. Nevertheless, the decrease of the $1/\nu$ transport leads to an increase of the stored energy.

Further improvement of the $1/\nu$ confinement properties can be achieved by reducing the parameter k_φ. In particular, in the case of identical currents in the TF coils for $k_\varphi \approx 0.31$ and the optimum $B_\perp$ value corresponding to some inward shift of the magnetic surfaces, the maximum in stored energy is 1.65 times higher than the corresponding maximum for $k_\varphi = 0.375$. These results are compatible with increased stability of the magnetic configuration with respect to additional distortions in the magnetic field.[18] Note that because of the scaling law [Eq. (7)], the same increase in the stored energy for a standard configuration would require 9.5 times higher input power P. Note also that for this k_φ a certain difference of currents in adjacent pairs of TF coils leads to an improvement of the $1/\nu$ transport in the same order of magnitude, too.

ACKNOWLEDGMENTS

This work has been partly carried out within the Association EURATOM-ÖAW and with funding from the Austrian Science Fund (FWF) under contract P16797-N08.

REFERENCES

1. O. S. PAVLICHENKO for U-2M GROUP, "First Results from the 'URAGAN-2M' Torsatron," *Plasma Phys. Control. Fusion*, **35**, B223 (1993).

2. V. V. NEMOV, S. V. KASILOV, W. KERNBICHLER, and M. F. HEYN, "Evaluation of $1/\nu$ Neoclassical Transport in Stellarators," *Phys. Plasmas*, **6**, 4622 (1999).

3. B. SEIWALD, V. V. NEMOV, S. V. KASILOV, and W. KERNBICHLER, "Optimization of Stellarators with Respect to Neoclassical Transport in Real Space," *Europhysics Conference Abstracts: 29th Conf. Plasma Physics and Controlled Fusion*, Montreux, Switzerland, June 17–21, 2002, Vol. 26B, p. P-4.099, European Physical Society (2002).

4. G. GRIEGER et al., *Phys. Fluids B*, **4**, 2081 (1992).

5. A. F. ALMAGRI, D. T. ANDERSON, S. F. B. ANDERSON, P. H. PROBERT, J. L. SHOHET, and J. N. TALMADGE, *IEEE Trans. Plasma Sci.*, **27**, 114 (1999).

6. A. REIMAN et al., *Phys. Plasmas*, **8**, 2083 (2001).

7. S. OKAMURA et al., *Europhysics Conference Abstracts, 27th Conf. Controlled Fusion and Plasma Physics*, Budapest, Hungary, June 12–16, 2000, p. P4.018, European Physical Society (2000).

8. S. OKAMURA et al., *Nucl. Fusion*, **39**, 1337 (1999).

9. S. MURAKAMI et al., *Nucl. Fusion*, **42**, L19 (2002).

10. O. MOTOJIMA et al., *Nucl. Fusion*, **43**, 1674 (2003).

11. H. E. MYNICK, *Phys. Fluids*, **26**, 1008 (1983).

12. C. D. BEIDLER et al., "Physics Studies for the Uragan-2M Torsatron," *Proc. 13th Conf. Nuclear Fusion*, Washington, D.C., Vol. 2, p. 663, International Atomic Energy Agency (1991).

13. V. E. BYKOV et al., "Optimization Study of Compact Torsatrons," *Proc. 12th Int. Conf. Plasma Physics and Controlled Nuclear Fusion Research 1988*, Nice, France, 1988, Vol. 2, p. 403, International Atomic Energy Agency (1989).

14. A. A. GALEEV and R. Z. SAGDEEV, in *Reviews of Plasma Physics*, Vol. 7, p. 257, M. A. LEONTOVICH, Ed., Consultants Bureau, New York (1979); see also in *Voprosy Teorii Plazmy*, Vol. 7, p. 205, Atomizdat, Moscow (1973) (in Russian).

15. V. E. BYKOV et al., *Fusion Technol.*, **17**, 140 (1990).

16. C. ALEJALDRE et al., "First Plasmas in the TJ-II Flexible Heliac," *Plasma Phys. Control. Fusion*, **41**, A539 (1999).

17. N. T. BESEDIN, G. G. LESNYAKOV, and I. M. PANKRATOV, *Voprosy Atomnoj Nauki i Tekhn., Ser. Termoyadernyj Sintez, Moskva*, No. 1, p. 48 (1991) (in Russian).

18. G. G. LESNYAKOV, D. D. POGOZHEV, Yu. K. KUZNETSOV, N. T. BESEDIN, E. D. VOLKOV, and O. S. PAVLICHENKO, "Studies of Magnetic Surfaces in the 'Uragan-2M' Torsatron," *Europhysics Conference Abstracts: 23rd Conf. Controlled Fusion and Plasma Physics*, Kiev, Ukraine, June 24–28, 1996, Vol. 20C, part II, p. 547, European Physical Society (1996).